IMPACT OF A SKEWED INLET BOUNDARY LAYER ON THE AERODYNAMIC PERFORMANCE OF A STATOR-HUB EQUIVALENT HIGH-TURNING COMPRESSOR CASCADE

Christoph BODE[1], Udo STARK[2], Nima FARD AFSHAR[1]

[1] *Institute of Jet Propulsion and Turbomachinery, Technische Universität Braunschweig, Hermann-Blenk-Str. 37, 38108 Braunschweig, Germany*

[2] *Institute of Fluid Mechanics, Technische Universität Braunschweig, Hermann-Blenk-Str. 37, 38108 Braunschweig, Germany*

SUMMARY

The paper reports on numerical investigations into the effects of inlet boundary layer skew on the aerodynamic performance of a low aspect ratio, high turning compressor cascade. The cascade geometry corresponds to the hub section geometry of a low aspect ratio stator of a highly loaded single-stage axial-flow low-speed compressor (fan). The skewed cascade flow simulates the reenergized stator hub flow and brings about a much better performance with inlet skew than without. However, the performance improvements caused by a skewed inlet boundary layer decrease with increasing inlet angle.

INTRODUCTION

The relative motion of adjacent blade rows generates an endwall boundary layer which, relative to the downstream blade row, is generally skewed and reenergized (i.e. with all velocity vectors of nearly the same length). This is illustrated in Figure 1 for the particular case of a hub endwall flow in a single-stage axial-flow low-speed compressor (fan). A collateral (2D) boundary layer leaves a rotor with large velocity deficiencies and enters the downstream stator with a highly skewed (3D) velocity profile of high kinetic energy. The rotor exit flow has been assumed collateral for reasons of simplicity. In general, however, the rotor exit flow is also skewed.

The direction of the skew is such that the endwall flow on hub and casing approaches the stator blades at high positive incidence angles. Assuming two-dimensional cascade flow, very high leading edge loadings with detrimental effects on losses may be expected at the formerly mentioned high incidence angles. However, experimental low-speed compressor data suggest that real leading edge loadings are not nearly as severe as those predicted by two-dimensional calculations using

measured inlet flow angle distributions. This alleviation is known as three-dimensional relief and was first investigated by Wadia and Beacher [1].

Bettner and Elrod [2] investigated the highly skewed stator casing flow in a single stage axial-flow low-speed compressor at various tip clearance, stage-loading and casing roughness conditions. The results show that tip clearance and stage loading variations exert a strong influence on overall performance and casing boundary layer growth. The influence of roughness variations on performance and boundary layer characteristics is altogether rather small. Predictions of the streamwise and normal boundary layer thicknesses with an endwall boundary layer method turned out to be a difficult task, see Elrod and Bettner [3] and De Ruyck and Hirsch [4].

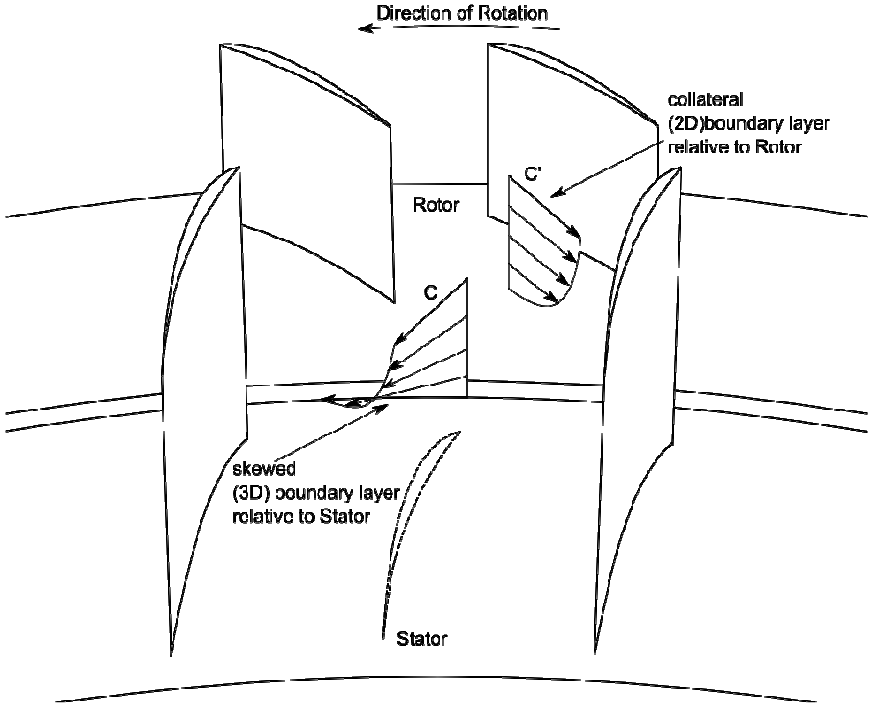

Figure 1: Velocity profiles in the hub region of a single-stage axial-flow fan

Flow conditions similar to those in single-stage stators may also be produced in linear compressor cascades using a moving belt or some other means to simulate a skewed inlet boundary layer. This, however, has rarely been done with the consequence that there is very little reported work on skew effects in compressor cascades. One exception, the authors found in the open literature, is a paper written by Moore and Richardson [5] who investigated a simulated rotor hub flow in a linear compressor cascade using air jets to produce a skewed inlet boundary layer. The mainly experimental results show the development of a three-dimensional endwall boundary layer along a free streamline midway between two blades under the influence of skew.

Nowadays CFD may be used to predict inlet skew effects on endwall flow phenomena and losses. In this sense Böhle and Stark [6] investigated a high turning stator cascade with and without skew, unfortunately for one inlet angle only. The more important results of this investigation may be summarized as follows: i) there was no leading edge separation in spite of very high incidence angles next to the endwalls, ii) the overturning of the endwall flow was less with inlet skew than without thus indicating a passage vortex of reduced strength, iii) due to ii), the interaction between the overturned endwall flow and the blade suction surface flow was less with inlet skew than without resulting in lower net total pressure losses and iv) the spanwise distribution of the losses and turning angles was more uniform when the inlet boundary layer was skewed.

These results are for one inlet angle only and may not be sufficient to create a sound understanding of inlet skew effects. With this in mind, the objectives of the present investigations were: i) to repeat and confirm the above mentioned results, ii) to continue to investigate the above mentioned compressor cascade at some additional inlet angles and iii) to analyze the numerical results for a better understanding of the inlet skew effects.

COMPRESSOR CASCACDE

The cascade geometry, cf. Figure 2, used for the present investigation corresponds to the hub section geometry of a low aspect ratio stator of a highly loaded single-stage axial-flow low-speed compressor[1]. The 2D designed blades were conventional compressor blades with a NACA 65 thickness distribution (d/l = 0.08) superimposed on a circular arc camber line (φ = 64.5°). The blade aspect ratio was h/l = 1.0, the space/chord ratio t/l = 0.5 and the stagger angle λ = 25°. The design inlet and outlet angle, β_1 and β_2, were at 54° and 4° respectively. The corresponding diffusion factor DF was 0.6, the ultimative diffusion limit for 2D compressor cascades. The endwall boundary layers in front of the cascade, cf. Figure 2, were assumed collateral or skewed.

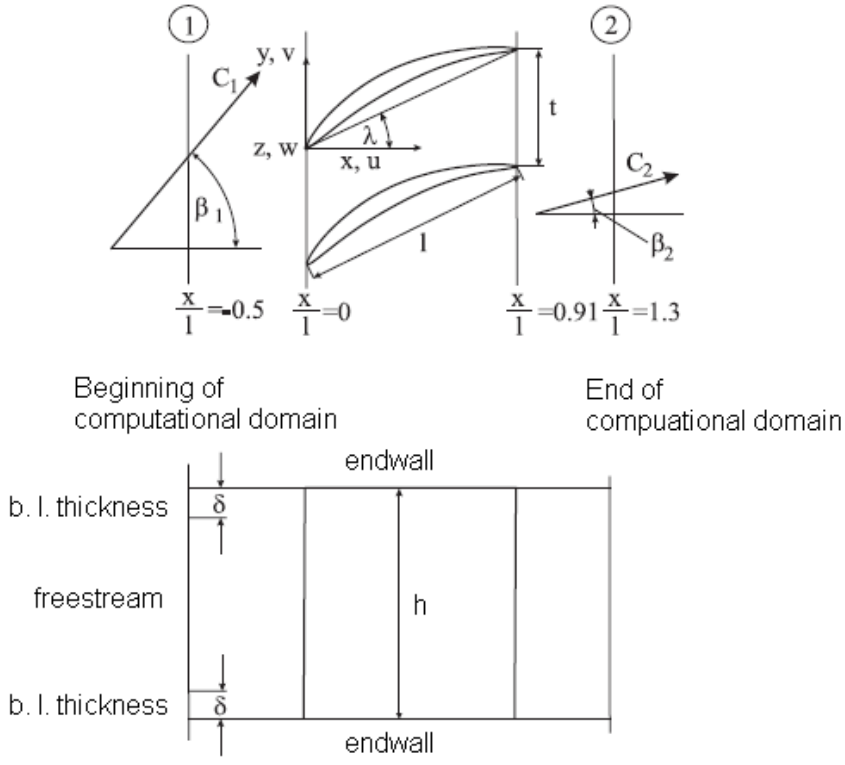

Figure 2: High turning compressor cascade with computational domain

NUMERICAL METHOD

All simulations of the present investigations were done with the commercially available steady three-dimensional RANS solver CFX 14.5 of ANSYS. Preliminary simulations were performed with different turbulence and transition models, along with a grid sensitivity analysis. The shear stress transport (SST) k-ω turbulence model [7] turned out to be best suited for the present investigation with a focus on turbulent endwall and secondary flows. The computational domain

[1] $\varphi = 0.4$; $\psi = 0.55$; $\psi_{th} = 0.65$; $\nu = 0.55$

covered one blade passage between periodic boundaries on top and bottom and two additional boundaries at 50% true chord axial upstream and 40% true chord axial downstream of the cascade, cf. Figure 2. In order to limit the grid size, only one half of the blade span was meshed, using a mirror boundary condition at midspan. Computational grids of increasing number of cells were generated using the commercial grid generator ICEM-CFD of ANSYS. The following sensitivity analysis showed that at least 2.2 million cells were required to achieve i) a high resolution of the boundary layers with $y^+ \approx 1$ and ii) the overall performance parameters accurately. The solution was assumed to have converged when the different RMS residuals reached a stable level, say less than 10^{-6}, and the relative difference of in- and outlet mass flow was less than 10^{-3}.

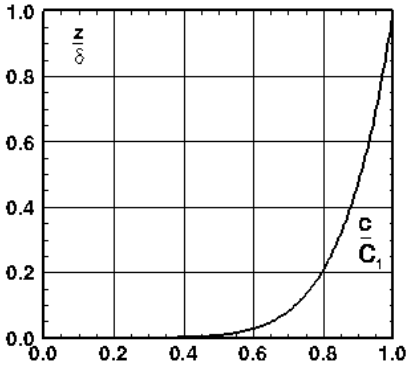

Figure 3: 2D Inlet boundary layer profile

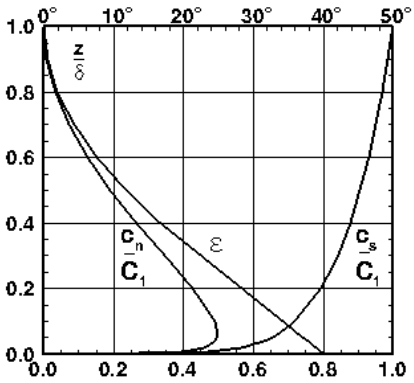

Figure 4: 3D Inlet boundary layer components

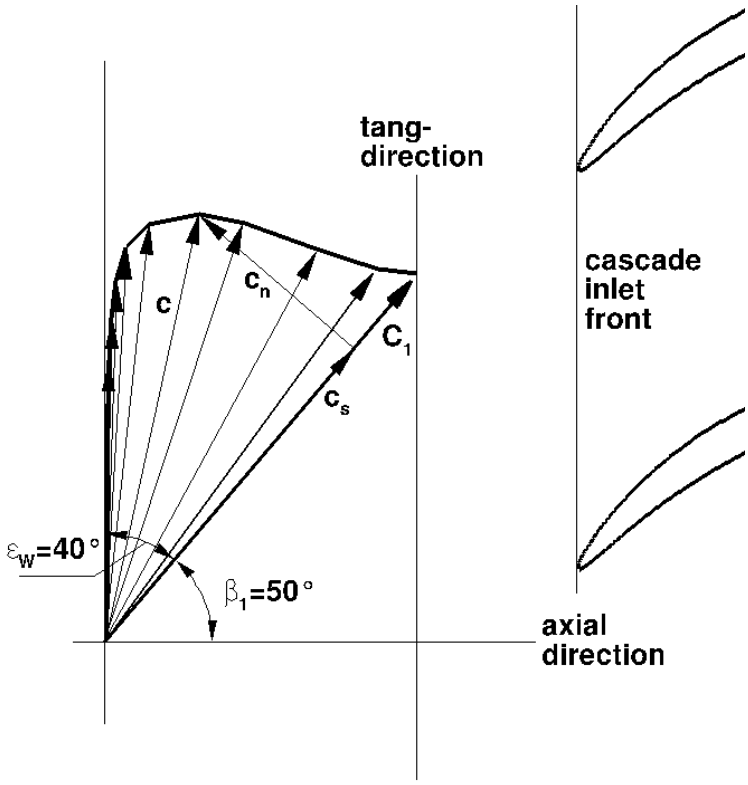

Figure 5: Velocity vectors of the skewed inlet boundary layer at x/l = -0.5

All simulations were done at a Reynolds number of $Re_1 = 5x10^5$ and a Mach number of $Ma_1 = 0.2$. At the inlet of the computational domain the total flow conditions ($T_{t1} = 300K$, $p_{t1} = 100\ 570$ Pa), the flow angles ($\beta_1 = 50$, 54 and 58°) and the turbulence intensity (Tu = 2%) were specified. At the outlet, the static pressure was prescribed and adjusted until the specified inlet conditions were matched. In addition, two inlet boundary layer velocity profiles were chosen to complete two total pressure profiles. The first one was a collateral velocity profile

$$\frac{c}{C_1} = \left(\frac{z}{\delta}\right)^{1/7} \tag{1}$$

As shown in Figure 3. The second one was a highly skewed velocity profile with components

$$\frac{c_s}{C_1} = \left(\frac{z}{\delta}\right)^{1/7} \tag{2}$$

and

$$\frac{c_n}{C_1} = \left(\frac{z}{\delta}\right)^{1/7}\left(1-\frac{z}{\delta}\right)^2 \tan(\varepsilon_W) \tag{3}$$

in streamwise and normal direction, cf. Figure 4 and 5. The corresponding flow angles $\beta_1(z)$ increased from $\beta_1 = 50°$, 54° and 58° at $z = \delta$ ($\delta/l = 0.1$) to $\beta_1 = 90°$ at the wall ($z = 0$), where the skewing angle ε became a maximum, i.e. $\varepsilon_W = 40°$, 36° and 32° respectively. Comparing the results, as detailed below, it was possible to clarify the impact of a skewed inlet boundary layer on the aerodynamic performance of compressor cascades.

RESULTS AND DISCUSSION

Wall Streamlines on Endwalls and Blades

Wall streamlines or skin-friction lines may be used to analyze the surface flow on blade profiles and endwalls. Following the criteria described by Perry and Fairlie [8], Tobak and Peake [9], Perry and Chong [10] and others, the more important features of surface flows may be summarized as follows:

i) Three-dimensional separation lines (convergence of the wall streamlines),

ii) Three-dimensional (re)attachment lines (divergence of the wall streamlines),

iii) Singular points (saddle points and nodes including nodal points and foci of attachment or separation)

The following definitions of singular points are due to Tobak and Peake and may be found in [9]:

i) A saddle point is a singular point where two particular skin-friction lines intersect. The directions on either side of the singular point are inward on one particular line and outward on the other particular line. All of the other skin-friction lines miss the singular point and take directions consistent with the directions of the adjacent particular lines.

ii) A nodal point is a singular point common to an infinite number of skin-friction lines. At that point all of the skin-friction lines except one are tangential to a single line.

iii) A focus differs from a nodal point in that it has no common tangent line. An infinite number of skin-friction lines spiral around the singular point, either away from it or into it.

These features, when identified, may be used to develop a first idea of the three-dimensional flow next to the surface under consideration. This concept has been used many times before, among others by Friedrichs et al. [11], who investigated three-dimensional stator hub boundary layer separations in two highly loaded single-stage low-speed compressors of low hub to tip ratio. A more recent study was performed by Gbadebo et al. [12], who investigated, experimentally and numerically, three-dimensional separations in two moderately loaded compressor cascades.

Wall streamlines and skin-friction contours are shown in Figure 6 and Figure 7 for case one and two with a collateral and a skewed inlet boundary layer respectively. The midspan inlet angle is $\beta_1 = 54°$ in both cases and represents design flow conditions. For well known reasons, the endwall flow is overturned in Figure 6 as well as in Figure 7. However, the overturning with skew in Figure 7 is smaller than without skew in Figure 6. This may be seen by comparing Figure 6 and 7 or, more clearly, by comparing the pitch averaged endwall streamline directions $\bar{\beta}(x/l_{ax})$ presented in

Figure 8. As a consequence, the following interaction between the overturned endwall flow and the suction surface flow is stronger in Figure 6 than in Figure 7, taking the spanwise penetration of the endwall flow into the suction side flow as an indication. In both cases the interaction starts at both ends of a blade at a singular point S1 (saddle point) on the suction surface at about 22% and 33% axial chord respectively. The interaction then spreads out downstream the suction surface separation lines originating at their respective saddle points and terminating at two foci in Figure 6 and a nodal point in Figure 7.

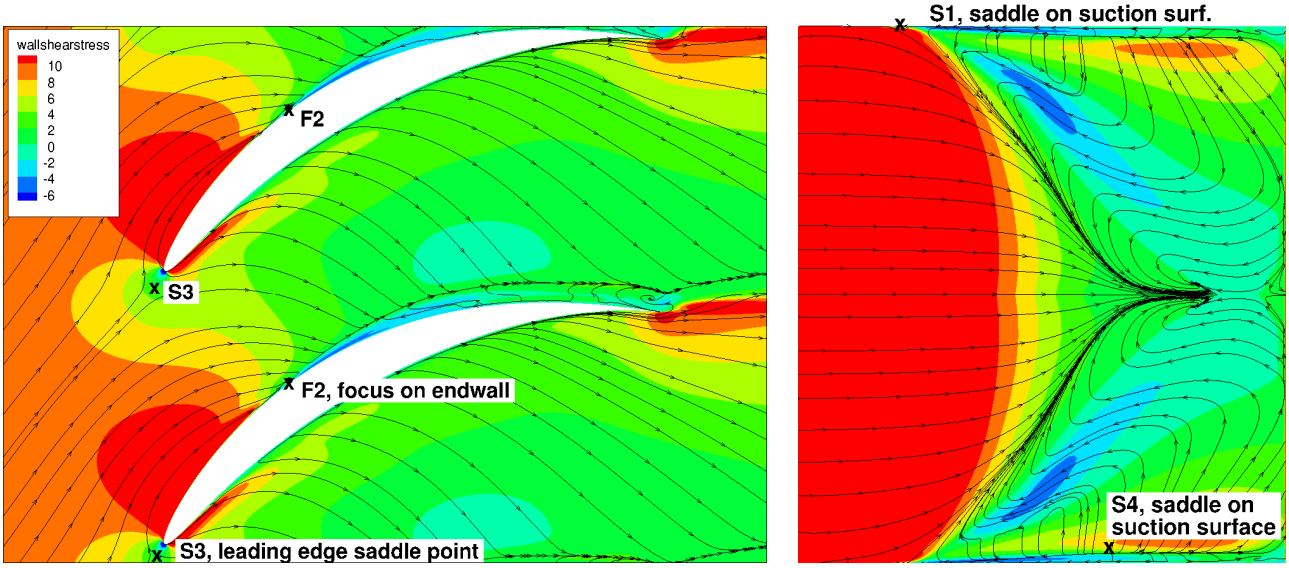

Figure 6: Wall streamlines and skin-friction contours for case one with collateral inlet boundary layer at $\beta_1 = 54°$

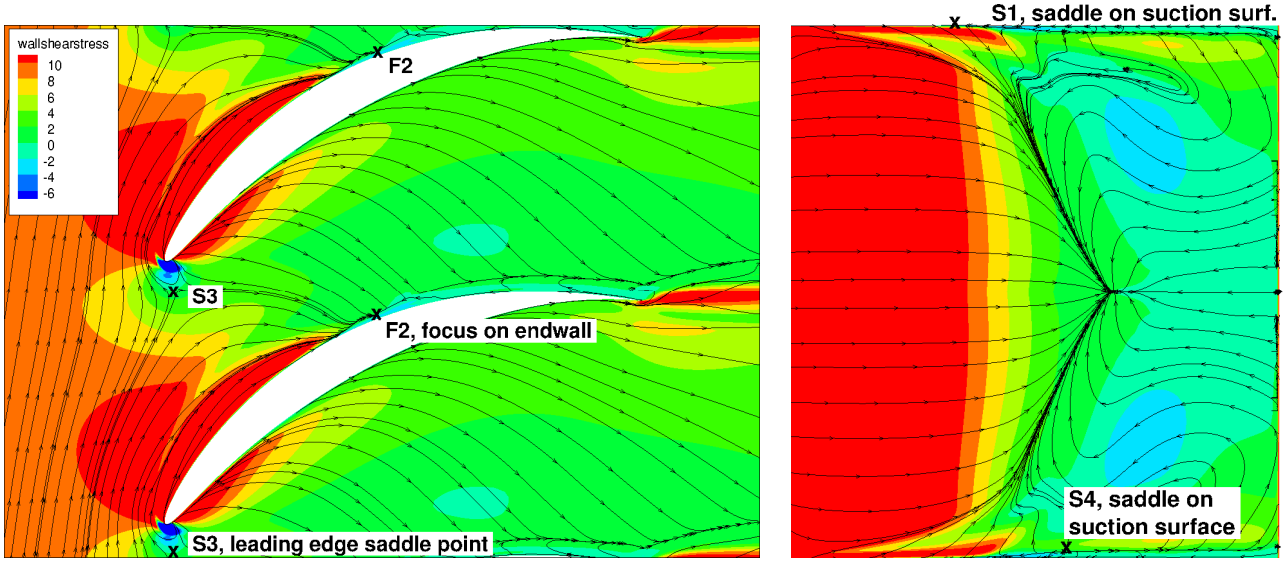

Figure 7: Wall streamlines and skin-friction contours for case two with skewed inlet boundary layer at $\beta_1 = 54°$

A blown up representation of the singular points and their immediate environs is shown in Figure 9 with S2, F1 and Figure 10 with N1 respectively. Downstream the separation lines the suction surface flow may be seen to be widely reversed, in Figure 6 as well as in Figure 7. The corresponding shear stresses are negative, partly higher in Figure 6 (collateral inlet boundary layer) than in Figure 7 (skewed inlet boundary layer). The mentioned saddle points S1 were also found by Gbadebo et al. [12]. His saddle points, however, were closely coupled with nodal points on the

endwalls, thus forming so called multiple singular points, which have not been found in the present results.

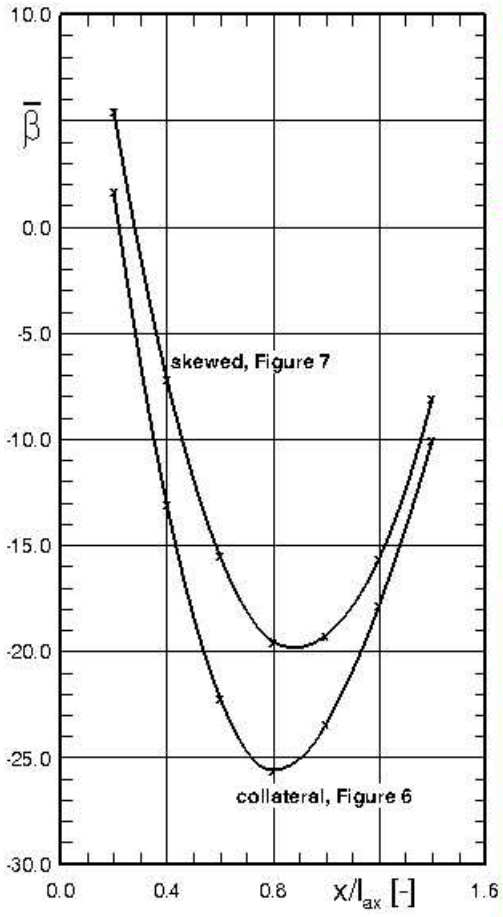

Figure 8: Pitch averaged wall streamline directions $\bar{\beta}(x/l_{ax})$ for case one and two without and with inlet skew at $\beta_1 = 54°$

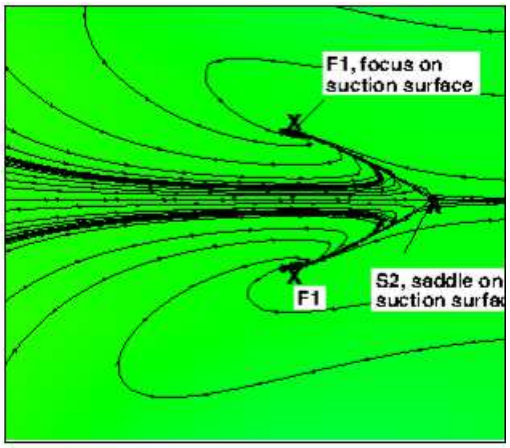

Figure 9: Details of the suction surface separation line for case one without inlet skew at $\beta_1 = 54°$

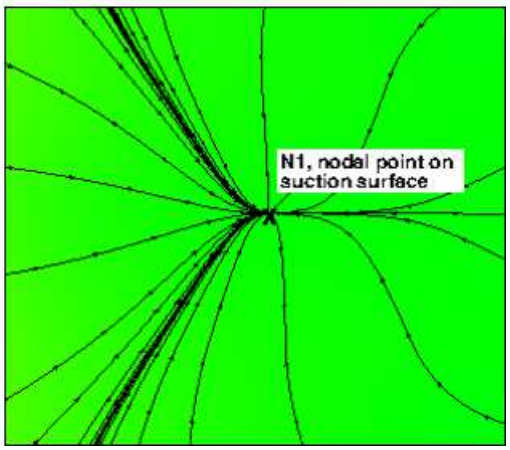

Figure 10: Details of the suction surface separation line for case two with inlet skew at $\beta_1 = 54°$

Two more streamlines of importance in Figure 6 and Figure 7 shall be mentioned and described. The first one is an endwall separation line and the second one a suction surface attachment line. The first line originates at the leading edge saddle point S3 and consists of two legs, a pressure and suction side leg, forming the base of the well-known horse-shoe vortex. Downstream the leading edge saddle point, the convergence of the wall streamlines becomes significantly weaker and the separation line is rather a dividing streamline than a separation line. This may be seen to change when the dividing streamline contacts the profile for a short distance at about 22% and 33% axial chord[2] in Figure 6 and 7 for case one and two respectively. In both cases the separation line continues downstream, lifts off the profile and winds into a focus F2 at about 25% and 43% axial chord as shown in Figure 11 and 12. Downstream the focus the separation line is upstream directed for a short distance between the focus F2 and the following saddle point S4. From there, however, the complete rest of the line is downstream directed.

The above mentioned second wall streamline is a suction surface attachment line running parallel to the suction surface | endwall corner at a small distance to the endwall. A saddle point S4 on the attachment line at about 62% and 56% axial chord in Figure 6 and 7 respectively, marks a particular

[2] The beginning of the suction surface separation lines S1

point where the attachment line direction changes from upstream (backward) to downstream (forward). The wall streamlines inside the suction surface endwall corner may be seen to be predominantly upstream (backward) directed.

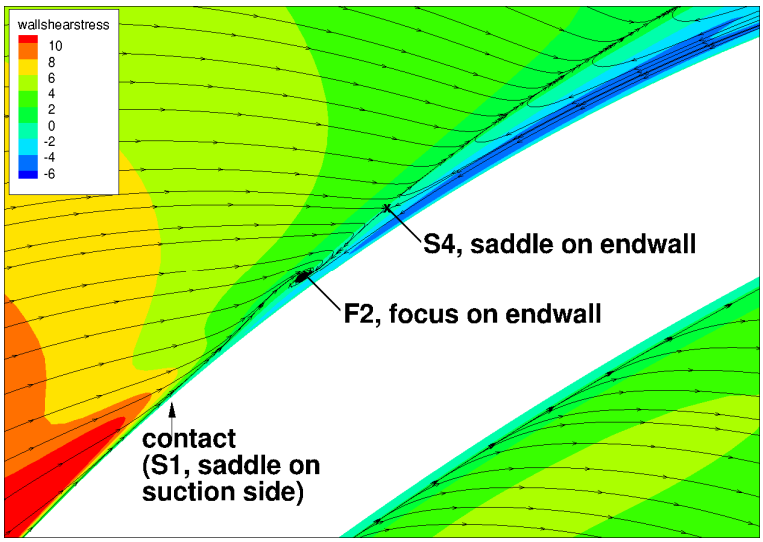

Figure 11: Endwall | suction side corner flow for case one with collateral inlet boundary layer at $\beta_1 = 54$

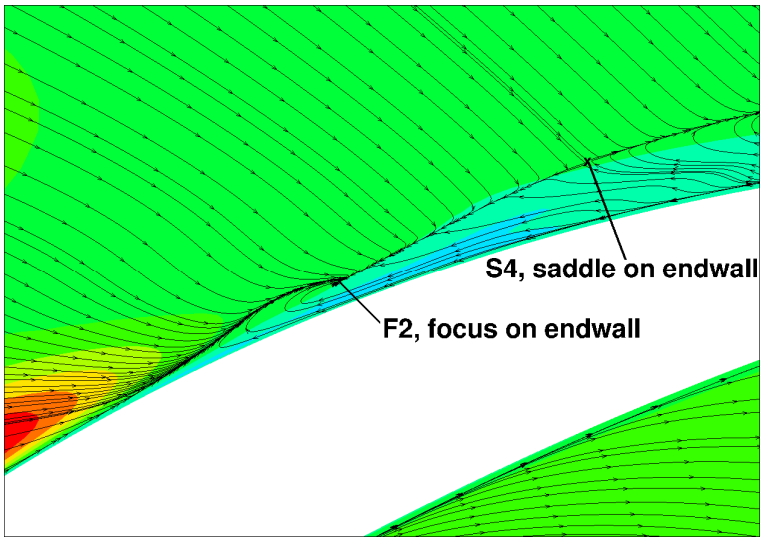

Figure 12: Endwall | suction side corner flow for case two with skewed inlet boundary layer at $\beta_1 = 54$

Because of the similarity between skin-friction lines and streamlines close to a wall, it may be realized that the incidence angles are much higher in Figure 7 than in Figure 6. This is due to the skewed inlet boundary layer and has been expected. A 2D analysis of the blade sections close to the endwall would probably indicate leading edge separation with detrimental effects on losses. This is definitely not the case in a 3D analysis as shown in Figure 7 with $\beta_1 = 54°$, the design inlet angle. This perplexing (Cumpsty [13]) phenomenon is known as three-dimensional relief (Wadia and Beacher [1]) and is by no means self-explanatory. For inlet angles somewhat higher than design, it may be shown that the leading edge flow slowly begins to deteriorate.

Local Results

Numerical data were acquired for a series of successive y/z-planes along the x-axis. The last y/z-plane coincides with the exit plane of the computational domain at x/l = 1.3. For this plane, Figure 13 and 14 presents contour plots of the normalized total pressure losses ζ_{V1} for case one and two

with a collateral and a skewed inlet boundary layer respectively. Results are shown for three inlet angles per case, including the design inlet angle $\beta_1 = 54°$. The total pressure losses are determined relative to the inlet total pressure p_{t1} at midspan and subsequently normalized with the corresponding dynamic head $q_1 = p_{t1} - p_1$.

The high blade loading of the present cascade results in suction side flow separation, flow reversal and high losses, cf. Figure 13 and 14. However, the losses shown in Figure 14 for case two with inlet skew are notably lower than the corresponding losses in Figure 13 for case one without inlet skew. This is an inlet boundary layer effect and may be explained as follows: i) The losses shown in Figure 13 and 14 include the inlet boundary layer losses, which are known to be much lower for a skewed boundary layer than for a boundary layer without skew. The interaction of the overturned endwall flow and the separated suction surface flow is much weaker with inlet skew than without. The losses produced inside the cascade (passage) are therefore lower in the second case than in the first one, as explained below. This has already been found by Böhle and Stark [6], although for only one inlet angle.

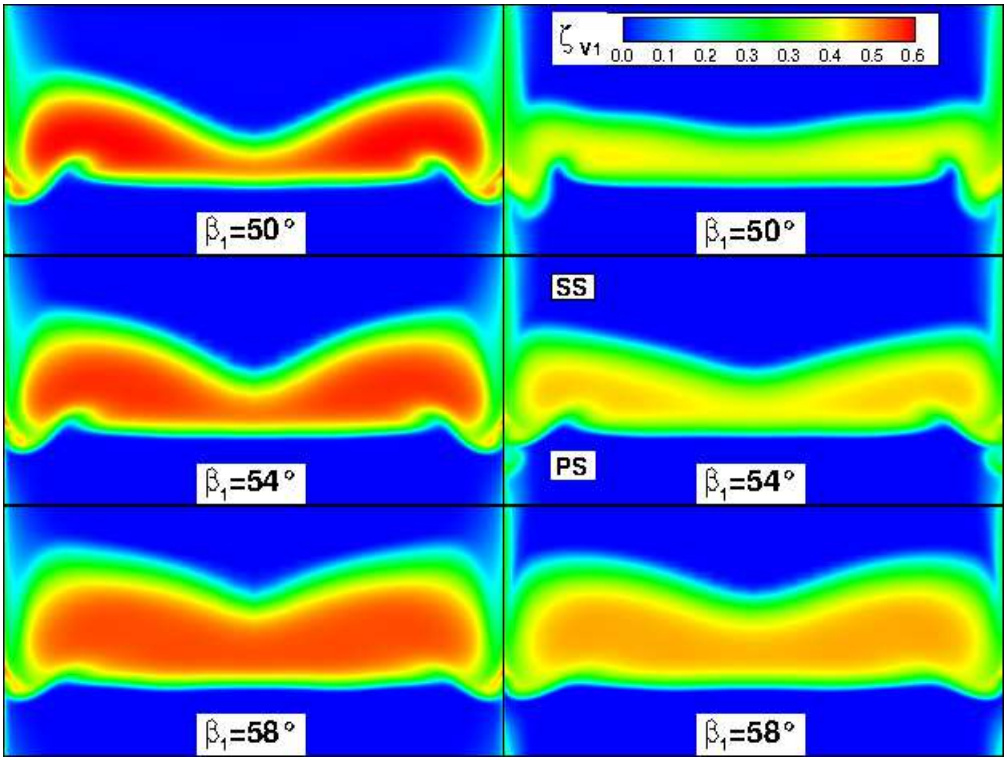

Figure 13: Total pressure loss contours for case one with a collateral inlet boundary layer

Figure 14: Total pressure loss contours for case two with a skewed inlet boundary layer

Pitchwise Averaged Results

Figure 15 shows the spanwise distribution of the pitchwise mass averaged loss coefficients $\bar{\zeta}_{V1}$ for case one and two at three inlet air angles. A similar presentation of the outlet air angle $\bar{\beta}_2$ is shown in Figure 16. In both figures the corresponding 2D results have been included for comparative purposes.

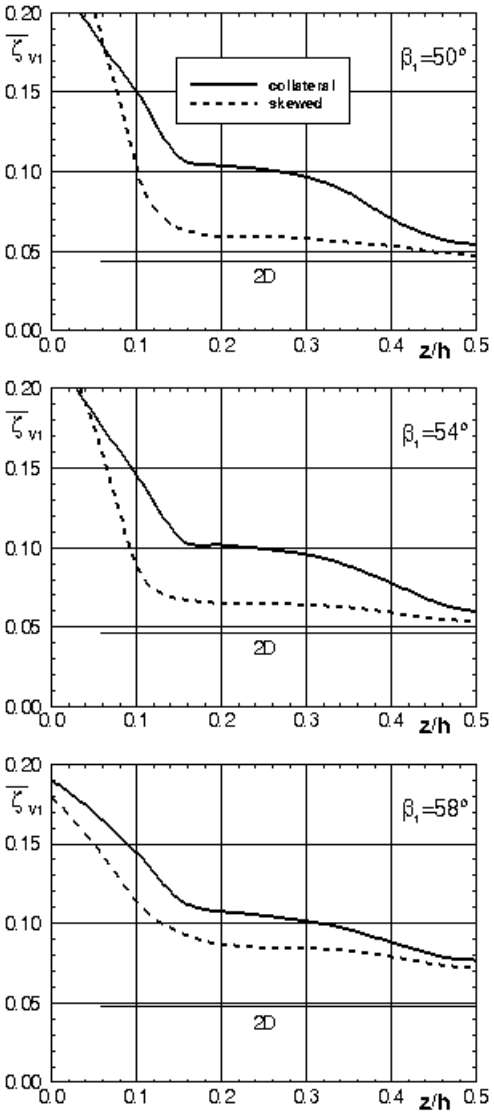

Figure 15: Pitchwise averaged total pressure losses for case one and two, x/l = 1.3

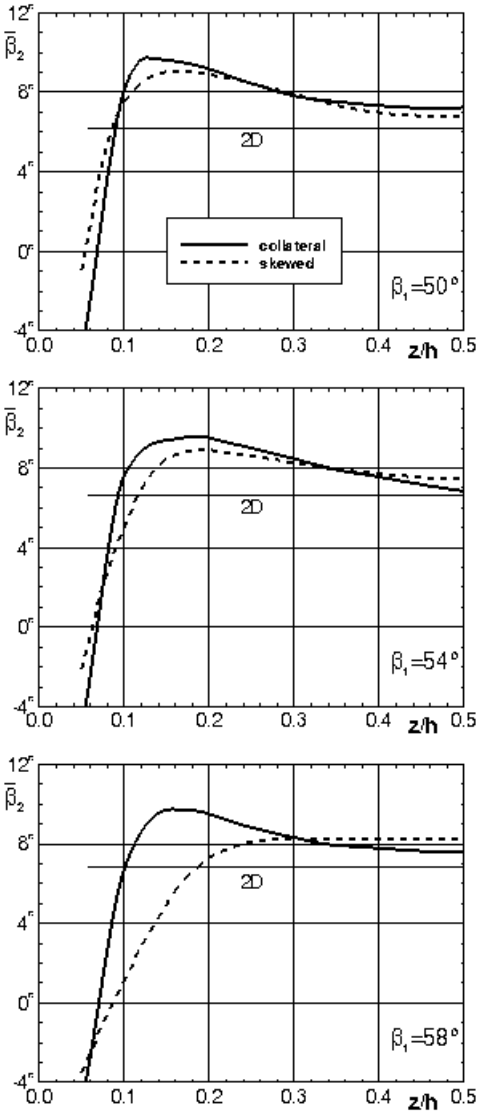

Figure 16: Pitchwise averaged outlet air angle for case one and two, x/l = 1.3

Although most of the work on linear cascades has been performed with collateral upstream endwall boundary layers, a few authors, Moore and Richardson [5], and Böhle and Stark [6] have examined the effects of skewed endwall boundary layers. These are expected to occur in real fans (and compressors) with the direction of skew such that the boundary layer flow approaches the blades at high positive incidence. The results presented in Figure 15 and 16 show that this has significant effects on losses and exit air angles. With few exceptions, the pitchwise averaged losses of case two with skew effects are substantially lower than the corresponding losses of case one without skew effects. This is in principle the same result as before and has been expected. A new finding, however, and difficult to make out in Figure 13 and 14, is the general decrease of the differences between case - one and - two losses with increasing inlet angle. For all three inlet angles, the corresponding exit angle distributions in Figure 16 show the classical overturning | underturning of the exit flow, somewhat less pronounced with inlet skew than without.

Pitch- and Spanwise Averaged Results

Pitch- and spanwise averaged loss coefficients $\overline{\overline{\zeta}}_{V1}$ for case one and two are shown in Figure 17 as a function of the normalized axial coordinate x/l between -0.5 and +1.3 at three inlet air angles β_1 = 50°, 54° and 58°. The two upper curves in the three diagrams of Figure 17 represent the

overall losses including both the inlet boundary layer losses ($x/l < 0$) and the cascade or passage losses ($x/l > 0$) for case one (solid lines) and case two (dashed lines) respectively. The reenergized inlet boundary layer of case two shows significantly lower losses when compared to the corresponding case one losses. Downstream the leading edge plane ($x/l = 0$), the overall losses increase rapidly in both cases and continue to increase downstream of the trailing edge plane ($x/l \sim 0.9$).

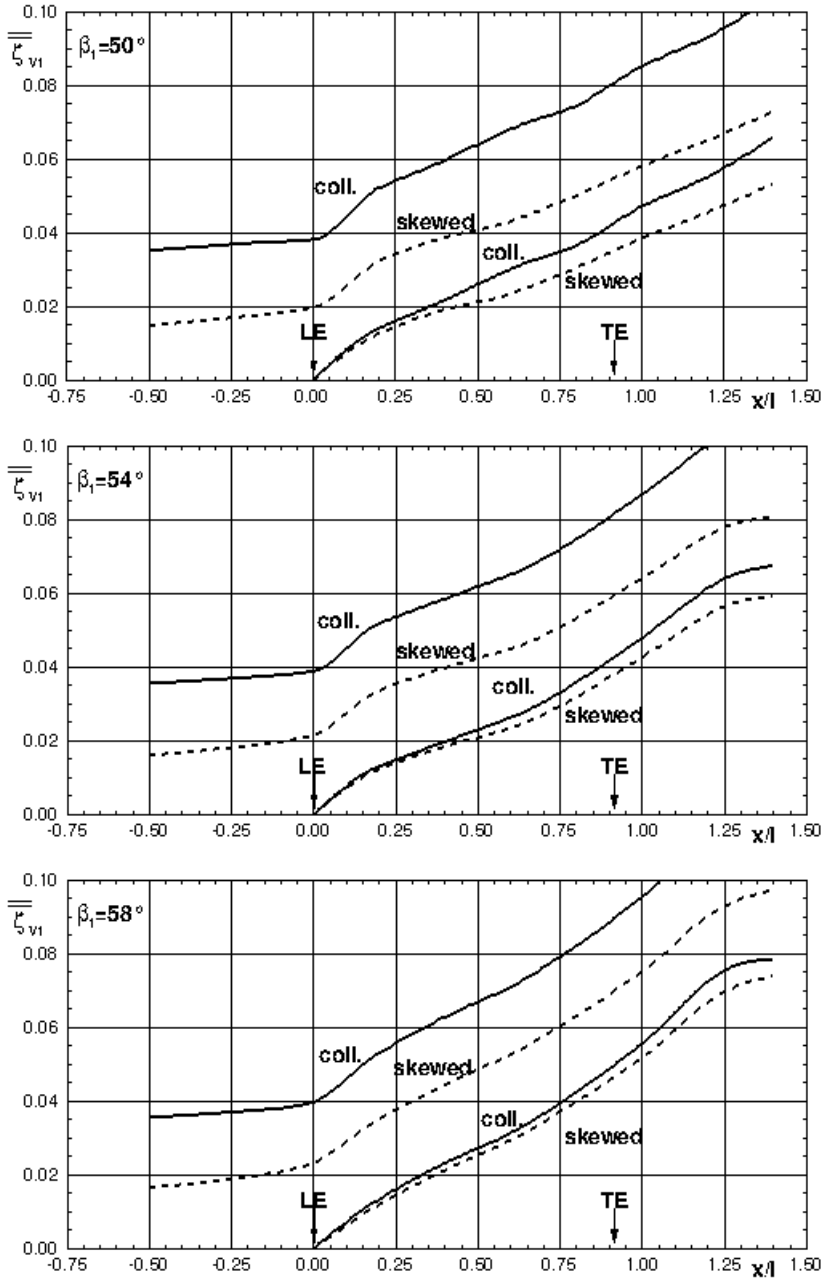

Figure 17: Pitch- and spanwise averaged total pressure losses, case one and two, β_1= 50, 54 and 58°

The two times three (six) lower curves in Figure 17 show the pure cascade or passage losses for case one and two. These curves were derived from the overall loss curves by subtracting the inlet boundary layer loss for case one and two at x/l = 0 from the corresponding overall loss curve. The resulting loss curves, with the case two losses always below the case one losses, show an increasing difference with x/l for all three inlet angles β_1= 50°, 54° and 58°. However, these differences decrease with increasing inlet angle. Their respective differences at x/l = 1 are 20%, 12% and 6% of the case one losses.

CONCLUSION

In axial fans and compressors the relative motion between adjacent blade rows causes the endwall boundary layers to be skewed and reenergized (i.e. with all velocity vectors of nearly the same length). This phenomenon has been investigated numerically in a simplified manner using a linear cascade model with collateral and skewed boundary layers on the upstream endwalls. The linear cascade geometry corresponds to the hub section geometry of a low aspect ratio stator of a highly loaded single-stage axial-flow low-speed compressor (fan).

All simulations were done with the commercially available, steady three-dimensional RANS solver CFX 14.5 of ANSYS. Preliminary simulations were performed with different turbulence and transition models, along with a grid sensitivity analysis[3]. The shear stress transport (SST) k-ω turbulence model of Menter turned out to be best suited for the present investigation focusing on turbulent endwall flows. The more important results of the investigation may be summarized as follows:

i) Wall streamlines or skin friction lines were generated and used to analyze the 3D surface flow on blade profiles and endwalls with both collateral and skewed boundary layers on the upstream endwalls. Well known criteria were applied to identify 3D separation and attachment lines as well as singular points.

ii) Extremely high inlet angles were found in the upstream boundary layers with skew. Based on two-dimensional thinking, a breakdown of the leading edge flow was expected but did not realize in a flow which is inherently three-dimensional.

iii) The overall losses, including the upstream endwall losses, were notably lower with inlet skew than without. The overall losses minus the upstream endwall losses (i.e. the passage losses) were again lower with inlet skew than without, not as much as before, but with interesting 20, 12 an 6% difference at $\beta_1 = 50°$, 54° and 58° and $x/l = 1$.

iv) Experimental investigations on passage (profile plus endwall) losses in linear cascades should be carried out with skewed boundary layers on the upstream endwalls in order to be as close as possible to the flow conditions in real fans.

BIBLIOGRAPHY

[1] A. R. Wadia, B. F. Beacher – *Three-Dimensional Relief in Turbomachinery Blading.* Journal of Turbomachinery, 112, pp. 587-596, **1990**.

[2] J. W. Bettner, C. W. Elrod – *The Influence of Tip Clearance, Stage Loading, and Wall Roughness on Compressor Casing Boundary Layer Development.* Journal of Engineering for Power, 105, pp. 280-287, **1983**.

[3] C. W. Elrod, J. W. Bettner – *Experimental Verification of an Endwall Boundary Layer Prediction Method.* AGARD-CP-351, pp. 25:1-21, **1983**.

[4] J. De Ruyck, C. Hirsch, P. Kool – *An Axial Compressor End-Wall Boundary Layer Calculation Method*. ASME Paper No. 78-GT-81, **1978**.

[5] R. W. Moore, Jr., D. W. Richardson – *Skewed Boundary Layer Flow Near the End Walls of a Compressor Cascade.* ASME Paper No. 56-A-131, **1956**.

[3] Not shown here because of space limitations

[6] M. Böhle, U. Stark – *A Numerical Investigation of the Effect of End-Wall Boundary Layer Skew on the Aerodynamic Performance of a Low Aspect Ratio, High Turning Compressor Cascade.* 7th European Turbomachinery Conference ETC 7, pp. 279-291, **2007**.

[7] F. R. Menter – *Two-Equation Eddy-Viscosity Turbulence Models for Engineering Applications.* AIAA Journal, 32, pp. 1598-1605, **1994**.

[8] A. E. Perry, B. D. Fairlie – *Critical Points in Flow Patterns.* Adv. Geophys., 18, pp. 299-315, **1974**.

[9] M. Tobak, D. J. Peake – *Topology of Three-Dimensional Separated Flows.* Ann. Rev. Fluid Mech., 14, pp. 61-85, **1982**.

[10] A. E. Perry, M. S. Chong – *A Description of Eddying Motions and Flow Patterns Using Critical-Point Concepts.* Ann. Rev. Fluid Mech., 19, pp. 125-155, **1987**.

[11] J. Friedrichs, S. Baumgarten, G. Kosyna, U. Stark – *Effect of Stator Design on Stator Boundary Layer Flow in a Highly Loaded Single-Stage Axial-Flow Low-Speed Compressor.* Journal of Turbomachinery, 123, pp. 483-489, **2001**.

[12] S. A. Gbadebo, N. A. Cumpsty, T. P. Hynes – *Three-Dimensional Separations in Axial Compressors.* Journal of Turbomachinery, 127, pp. 331-339, **2005**.

[13] N. A. Cumpsty – *Discussion to [1]*. Journal of Turbomachinery, 112, pp. 596-598, **1990**.